# Cu(II) and Gd(III) doped boehmite nanostructures: a comparative study of electrical property and thermal stability

Materials Research Express

PAPER

# Cu(II) and Gd(III) doped boehmite nanostructures: a comparative study of electrical property and thermal stability

**Shubham Roy**[1], **Souravi Bardhan**[1], **Dipak Kr Chanda**[2], **Anupam Maity**[3], **Saheli Ghosh**[1], **Dhananjoy Mondal**[1], **Subhankar Singh**[1] and **Sukhen Das**[1]

[1] Department of Physics, Jadavpur University, Kolkata-700032, India
[2] Advanced Materials and Mechanical Characterization Division, CSIR-Central Glass and Ceramics Research Institute, Kolkata- 700032, India
[3] School of Materials Science, Indian Association for the Cultivation of Science, Kolkata- 700032, India

**E-mail:** sdasphysics@gmail.com

**Keywords:** boehmite, ac conductivity, dielectric property, microstructure

OPEN ACCESS

RECEIVED
9 November 2019

REVISED
24 January 2020

ACCEPTED FOR PUBLICATION
29 January 2020

PUBLISHED
10 February 2020



## Abstract

The present article reports the effect of transition ($Cu^{2+}$) and rare earth metal ($Gd^{3+}$) ion doping on structural, microstructural and electrical properties of boehmite nanoparticles. Rietveld refinement is adopted here to refine the x-ray diffractograms for further analyzing the microstructural details and their alteration due to the incorporation of foreign cations. This is probably the first time when dielectric properties of these doped boehmite samples having been reported herein. These samples show remarkably high dielectric constant values which corroborate that doping enhances the microstrain values inside the orthorhombic structure and results in higher crystallographic defects. Enhancement in defect sites causes the augmentation of relative permittivity and ac conductivity. Temperature stability has also been enhanced significantly in our Cu-doped sample. The present study enables us to determine a relationship between crystalline deformation and electrical properties of nanomaterials which may be highly beneficial in fabricating cost-effective energy harvesting devices.

## 1. Introduction

Advancement of humankind put its giant footmark in every branch of science and technology and comes out with flourishing results like nanoscience and nanotechnology which enables us to go to any extent in material research that is still undiscovered. Nanotechnology and nanoscience is the pioneer of producing significantly promising nano-materials with applications in various fields of electronics [1, 2], catalysis [3–6], energy storage [7, 8], pharmaceutics and medical sciences [9–13]. Nowadays, researchers particularly focuses on multifunctional or hybrid nanomaterials those are having multiple areas of application. However, these multifunctional materials are either multi-crystalline or form a composite [7, 8]. Thus, a considerable amount of interest has been given nowadays for fabricating such nanocomposite or doped nanomaterial [14–16].

In spite of that, biocompatibility and bioavailability are major issues that determines the potential areas of application which is the main reason for the replacement of hazardous nanoparticles with biocompatible ones [17]. In recent times, some studies show that the researchers are focussing on biocompatible nano-systems to fabricate efficient and cost-effective organic solar cells [18], heavy metal sensors [19–21], gas sensors [22] and energy harvesting devices such as nanogenerators [23] and supercapacitors [24–26]. These next-generation nano-systems and nano-devices are capable to reduce environmental pollution and delivers greater efficiency [27, 28].

Boehmite ($\gamma$-AlOOH) is a typical oxy-hydroxide compound of aluminum with a layered orthorhombic structure [29, 30]. Previously, extensive research has been done on different synthesis pathways of this nanomaterial [31, 32]. Some research is based on different properties such as optical [33], electrical [34], mechanical properties [35] of boehmite those are showing its multi-dimensional usability. Biocompatibility is another major advantage of selecting boehmite for any application [36]. Boehmite was reported as a promising dental and orthopedic material due to its biocompatibility and bioavailability [37, 38]. Nonetheless, a very limited amount of interest has been paid on hybrid or doped boehmite nanostructure.

In this study, we have developed a transition metal (Cu(II)) and another rare earth metal (Gd(III)) derived boehmite nano-systems that are capable of producing remarkably high electrical permittivity and greater temperature stability (in case of the copper doped sample). The foreign metal ions are doped into the orthorhombic structure of boehmite matrix in a very small quantity (1% weight) and characterized by using x-ray Diffraction (XRD), FT-IR (Fourier Transform Infrared Spectroscopy), TEM (Transmission Electron Microscopy) and Brunauer–Emmett–Teller (BET). A detailed crystallographic analysis of the samples was done by refining the XRD patterns of the samples by using a Rietveld based software package MAUD and analyzed herein. Comprehensive dielectric and ac conductivity studies have been performed and analyzed to ascertain the alteration of electrical quality of the samples as a function of crystallographic deformation created by foreign metal ion mediated doping. Increasing temperature stability, extensively high dielectric value with a very low tangent loss makes these doped boehmite samples potential candidates for energy harvesting applications.

## 2. Experimental section

### 2.1. Materials

Aluminum nitrate nonahydrate [$Al(NO_3)3{\cdot}9H_2O$], aqueous ammonia solution (25%), copper acetate, acetone (HPLC grade) and ethanol (HPLC grade) were purchased from Merck, India while gadolinium oxide was purchased from SRL, India. All the reagents used were of analytical grade and were used without any further purification. Millipore water with a resistivity of at least 18.2 MΩ.cm was used throughout our experiments.

### 2.2. Synthesis

Nanostructures of doped and undoped boehmite samples were synthesized by a facile two step hydrothermal process. Undoped boehmite nanoparticles (NBH) were obtained by dissolving aluminum nitrate in 70 ml Millipore water using magnetic stirrer at room temperature followed by the drop-wise addition of ammonia solution until the pH reached at 10. In case of copper-doped boehmite (CBH) and gadolinium-doped boehmite (GBH), copper acetate and gadolinium oxide were added respectively into the solutions, maintaining the weight ratios of Cu and Gd to be 1%, followed by pH adjustment at 10 using ammonia solution. After proper dissolution through vigorous stirring for 3 h, the solutions were transferred into separate Teflon lined stainless steel autoclaves which were then placed in a dust free hot air oven at180 °C for 18 h.

The solid precipitates were collected from the bottom of each Teflon jacket, washed several times with Millipore water, dried in vacuum at room temperature, then ground using a mortar, marked and sent for further characterizations.

## 3. Results and discussion

### 3.1. Structural and microstructural analysis

X-Ray Diffraction (XRD) is an efficient and significant characterization tool for the determination of crystal size, structure, microstructure along with detection and quantification of phase purity [39]. To determine the crystallinity of our samples, an x-ray powder Diffractometer (XRD) (D8, Bruker AXS, Winconsin, USA) was employed using Cu-Kα target at the wavelength of 1.5418 Å and operated at 35 kV, 35 mA with a scan speed of 2 s/step and $2\theta$ range from 15°–60°. Structural and microstructural parameters were studied through the refinement of the obtained samples using Rietveld based MAUD program (version: 2.8), and the refined structures were theoretically constructed using the VESTA program (version: 3.4.3). Figure 1 depicts the XRD patterns of the synthesized samples superimposed with corresponding miller indices, which are found to be in good agreement with the Joint Committee on Powder Diffraction Standards (JCPDS) card no.21–1307. Absence of any extra undesirable peak confirms their purity and ascertain that both $Gd^{3+}$ and $Cu^{2+}$ ions in the case of GBH and CBH respectively do not alter the orthorhombic structure of boehmite even up to 1% doping and are successfully incorporated into the structure.

Rietveld refinement was performed for the undoped (NBH) and doped (CBH and GBH) samples to analyze their microstructural and structural characteristics [40]. There is a subsequent increase in microstrain on the addition of foreign $Gd^{3+}$ and $Cu^{2+}$ ions, which might be due to the substitution of smaller $Al^{3+}$ ions (0.53 Å) by larger $Gd^{3+}$ ions (0.94 Å) or $Cu^{2+}$ ions (0.71 Å) into the orthorhombic unit cells [41]. Besides that, entry of larger cation inside the lattice structure causes internal homogeneous lattice stress which is evident from the slight shifting of diffraction maxima towards the higher diffraction angle in the case of CBH and GBH [42]. Thus the dopants have created structural defects that can alter various physicochemical properties of boehmite. All structural and microstructural data obtained from the refinement for all the three samples are illustrated in table 1.

Detailed analysis of structural and bond properties was done by using Vesta v3.4.3 (Visualization for Electronic and Structural Analysis) software and have been depicted in figure 1. Incorporation of $Gd^{3+}$ and

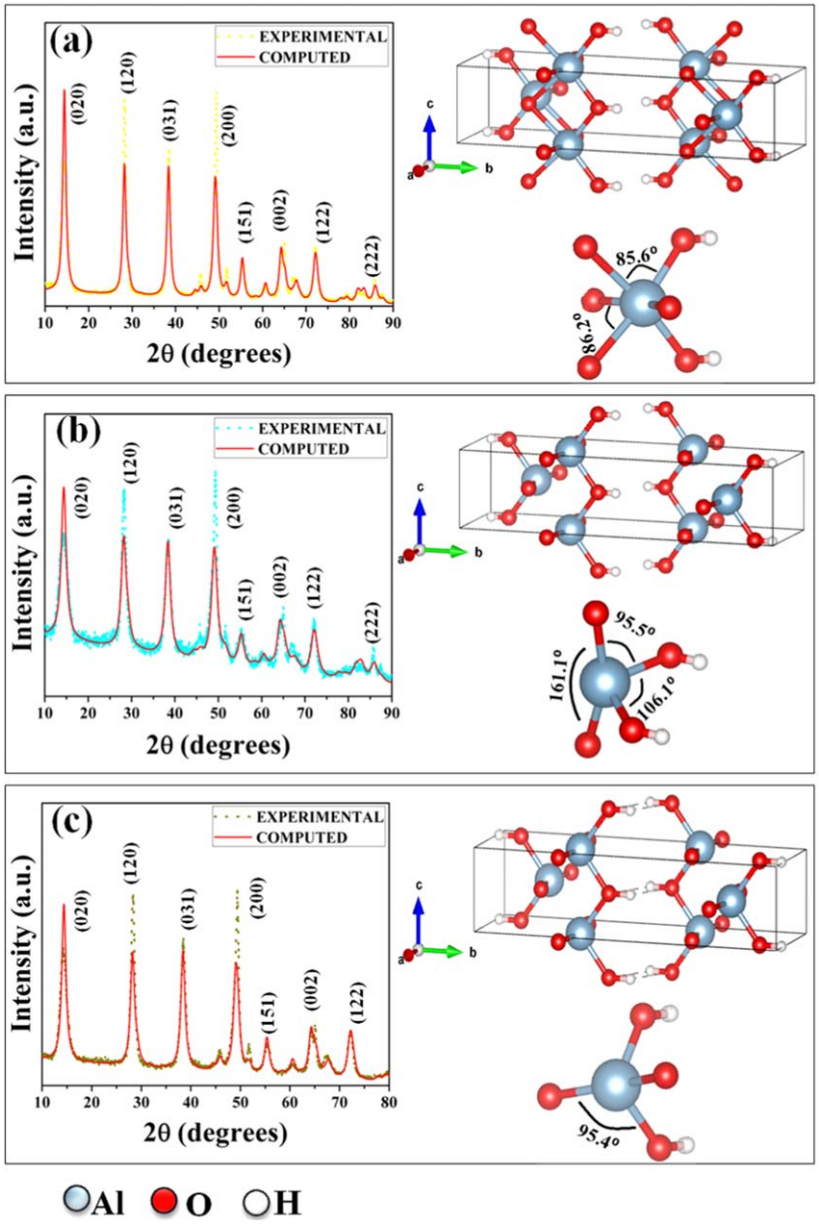


**Figure 1.** XRD patterns and corresponding microstructural diagrams of the samples (a) NBH, (b) GBH and (c) CBH.

**Table 1.** Structural and microstructural parameters of the samples obtained from Rietveld refinement of XRD diffractograms.

| Parameters | NBH | GBH | CBH |
|---|---|---|---|
| a (Å) | $3.69205 \pm 7.694 \times 10^{-4}$ | $3.6949866 \pm 0.0013171516$ | $3.688224 \pm 8.923 \times 10^{-4}$ |
| b (Å) | $12.210675 \pm 0.0033434944$ | $12.242514 \pm 0.0064571705$ | $12.226487 \pm 0.004935658$ |
| c (Å) | $2.8641748 \pm 5.9727 \times 10^{-4}$ | $2.8604217 \pm 0.0010346824$ | $2.8592756 \pm 7.333 \times 10^{-4}$ |
| nanocrystallite size (nm) | $12.583597 \pm 1.2386371$ | $7.7872505 \pm 0.72373766$ | $11.0133644 \pm 1.0858079$ |
| strain | $1.3950 \times 10^{-9}$ | $1.7313 \times 10^{-5}$ | $4.6784 \times 10^{-6}$ |
| $\chi^2$ | 1.6206 | 1.7689 | 1.6984 |
| $R_p$ (%) | 0.16076866 | 0.094971605 | 0.12739837 |
| $R_{wp}$ (%) | 0.20466273 | 0.12631688 | 0.16602717 |

$Cu^{2+}$ ion does not alter the structural symmetry but the stress created from substitution by larger ions ($Gd^{3+}$and $Cu^{2+}$) changes the bond angle (table 3) and bond lengths (table 2) slightly in case of GBH and CBH.

In order to ensure successful incorporation of $Gd^{3+}$ and $Cu^{2+}$ into the orthorhombic structure of boehmite, FT-IR spectroscopy was performed (figure 2) in a Shimadzu FTIR-8400S spectrometer in the wavenumber range from 400 $cm^{-1}$ to 4000 $cm^{-1}$ and 80 individual scans were taken and merged together to obtain the final spectra for

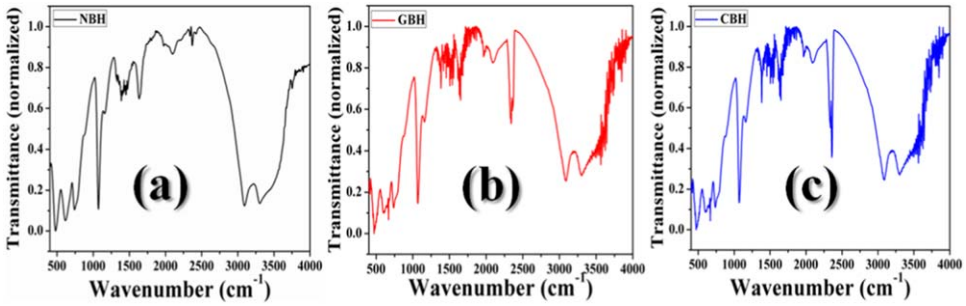


**Figure 2.** FTIR spectra of the samples (a) NBH, (b) GBH and (c) CBH.

**Table 2.** Variation of the bond lengths of pure and doped boehmite samples.

| Nature of the bond | NBH (Å) | GBH(Å) | CBH(Å) |
|---|---|---|---|
| Al–O ($O_1$) | 1.87386 | 1.87285 | 1.86532 |
| Al–OH ($O_2$) | 1.83549 | 1.78957 | 1.83252 |

**Table 3.** Variation of the bond angles of pure and doped boehmite samples.

| Angle between | NBH (degree) | GBH(degree) | CBH(degree) |
|---|---|---|---|
| OH–Al–O | 85.5992 | 95.6575 | 95.3984 |
| OH–Al–OH | 102.5614 | 106.1062 | 102.5486 |
| O–Al–O | 86.2401 | 161.1207 | 162.7013 |

each sample. 2 mg of each sample was homogenized with 100 mg KBr (at 1:50 ratio) and the mixtures were pressed for 5 min at 5 ton in a hydraulic hand press to form a 10 mm pellet which was dried at 80 °C for 4 h before measurement in order to remove excess moisture. Figure 2 depicts the FTIR spectra of as-synthesized nanostructures.

In the case of normal boehmite (NBH), the absorption peaks were located at 480, 758, and 634 $cm^{-1}$, which are the characteristic peaks of boehmite [43]. Small peaks located at 1069 and 1158 $cm^{-1}$ respectively were due to Al-O-H vibration [44]. Absorption bands located at 3095 and 3305 $cm^{-1}$ are due to symmetric and asymmetric O–H vibrations respectively [45]. The absorption band at 1634 $cm^{-1}$ is due to moisture adsorbed on the surfaces of the samples [46]. Moreover, GBH and CBH samples show a similar type of absorption band pattern which signifies that incorporation of the $Gd^{3+}$ and $Cu^{2+}$ neither alter any bond structure nor create any bonding network inside the boehmite phase, which agrees with our XRD results.

Detailed morphological features were analyzed by using a JEOL JEM-2000 transmission electron microscope (TEM) with an operating voltage of 200 kV. A minute amount of sample was well-dispersed in acetone, sonicated till the homogenous solution was formed, and then drop-casted on carbon-coated copper grids of 300 mesh for microscopy.

Doping-dependant alteration in morphological features of the three samples was investigated using TEM analysis which confirmed that there is a change in particle morphology resulting from subsequent addition of $Gd^{3+}$ and $Cu^{2+}$ ions in the structure (figure 3). In the case of the undoped sample (NBH), the particles appeared to be hexagonal with a sponge-like porous structure. Copper doped boehmite (CBH) sample shows highly porous rhomboidal morphology with a mean pore diameter of 2–4 nm. Rare earth gadolinium doped GBH particles appeared to be rod-like. Previously, we have mentioned in our article [38] that increasing microstrain changes the particle morphology significantly by virtue of crystal defects which contribute toward this morphological evolution [41]. Here, in the case of CBH, the ionic radius of copper ions is quite smaller than that of gadolinium ions. Thus, the microstrain created inside the orthorhombic structure of the host material in the case of CBH is also lower than that of GBH. Henceforth, the morphology has drastically been changed into rod-shaped, whereas, CBH sample has been completely transformed into rhomboidal particles. Moreover, the incorporation of foreign cations inside the pure boehmite matrix have been examined and justified by using Energy Dispersive x-ray spectroscopy (EDX) (figure 4). The traces of Gd and Cu inside the orthorhombic phase

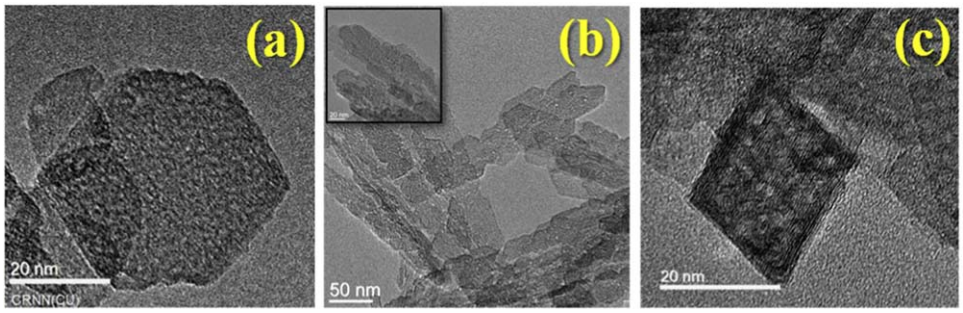


**Figure 3.** TEM micrographs of as-synthesized (a) NBH, (b) GBH and (c) CBH.

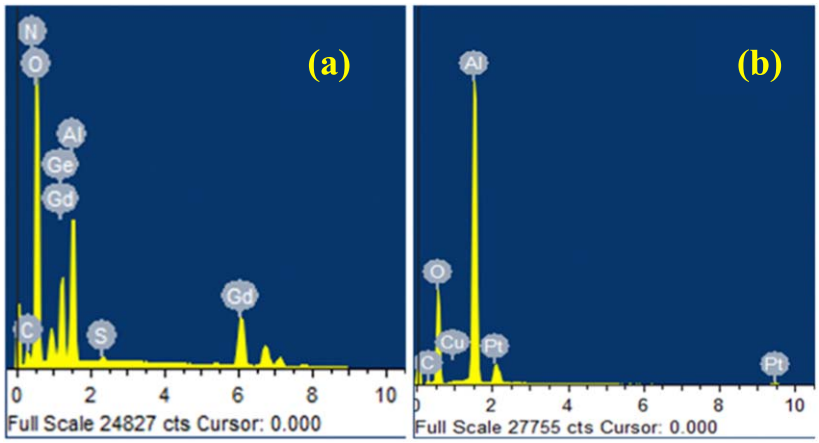


**Figure 4.** EDX spectra of (a) GBH and (b) CBH samples those are showing the traces of Gd and Cu respectively in the boehmite (γ-AlOOH) matrix.

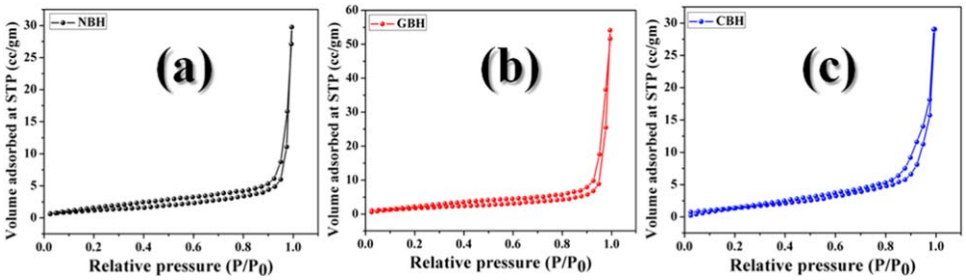


**Figure 5.** $N_2$ adsorption/desorption isotherm of (a) NBH, (b) GBH and (c) CBH.

of boehmite can be observed in EDX data which corroborates that the foreign impurities have been properly incorporated in the boehmite samples.

### 3.2. Surface area and porosity analysis

The pore size distribution and surface area of the as-synthesized nanostructures have been analyzed through Brunauer–Emmett–Teller (BET) and Barrer-Joyner-Halenda (BJH) methods by using $N_2$ gas adsorption-desorption values by employing a Twin Surface Area Analyzer from Quanta-chrome Instruments (USA).

Surface areas of the synthesized nanostructures corresponding to the nitrogen ($N_2$) adsorption-desorption isotherms and their corresponding pore size distributions are illustrated in figure 5. The type-IV isotherm (figure 6) obtained from the data indicates that the undoped (NBH) sample is mesoporous, having a pore diameter of 3.53 nm in our samples [47, 48]. H4-type hysteresis loops were obtained for all the samples,

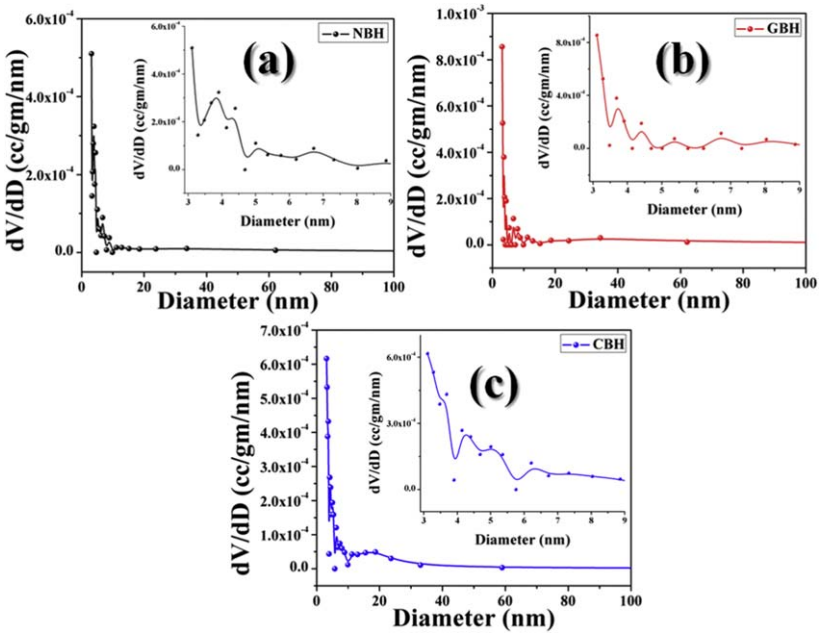


**Figure 6.** Pore size distribution data of (a) undoped NBH, (b) Gd-doped GBH and (c) Cu-doped CBH.

**Table 4.** Estimated BET surface area, pore radius and pore volume of pure and doped boehmite nanostructures.

| Sample name | Surface area ($m^2/g$) | Pore size (nm) | Pore volume (cc./g) |
|---|---|---|---|
| NBH | 4.473 | 3.530 | $4.292 \times 10^{-2}$ |
| GBH | 6.406 | 3.113 | $9.532 \times 10^{-2}$ |
| CBH | 5.282 | 3.113 | $4.514 \times 10^{-2}$ |

indicating the formation of slit-like pores [47, 48]. From the BET data, it is quite evident that the surface areas of the doped boehmite samples enhanced quite significantly. The surface area for NBH was found to be 4.473 $m^2\ g^{-1}$ while the surface area of CBH and GBH was found to be 5.282 $m^2\ g^{-1}$ and 6.406 $m^2\ g^{-1}$ respectively (table 4). This surface area enhancement could be beneficial for producing high dielectric materials.

### 3.3. Dielectric permittivity analysis

Electrical properties (dielectric constant and electrical conduction mechanism) were determined by using an Agilent 4294 A Precision Impedance Analyzer operating at 0.5 V bias voltages set at a frequency range from 40 Hz to 10 MHz. Solid pellets of the samples were prepared to compact them in the Hydraulic press system at 5 tons for 5 min, using small metallic sample holders and the sent for electrical characterizations.

Dielectric properties of a material can be described using the relation [49],

$$\varepsilon = \varepsilon' + j\,\varepsilon'' \tag{1}$$

where, $\varepsilon'$ and $\varepsilon''$ are the real and imaginary part of the relative dielectric constant respectively, and $\varepsilon'$ contributes to the quantity of energy stored in the material due to polarization effect and often referred as dielectric constant, whereas the imaginary part ($\varepsilon''$) is related to the energy dissipated by the material. The real part of the dielectric constant can be calculated using the relation:

$$\varepsilon' = \frac{C.d}{\varepsilon_0 \mathrm{A}} \tag{2}$$

where, C is the capacitance of the sample, d and A are thickness and surface area of the sample respectively and $\varepsilon_0$ is the permittivity of free space ($8.85 \times 10^{-12}$ F $m^{-1}$). Doping dependent variation of the real part of the dielectric constant ($\varepsilon'$) with applied field frequency (ranging from 40 Hz to 10 MHz) at different temperatures ranging from 30 °C to 150 °C has been shown in figures 7(a)–(c).

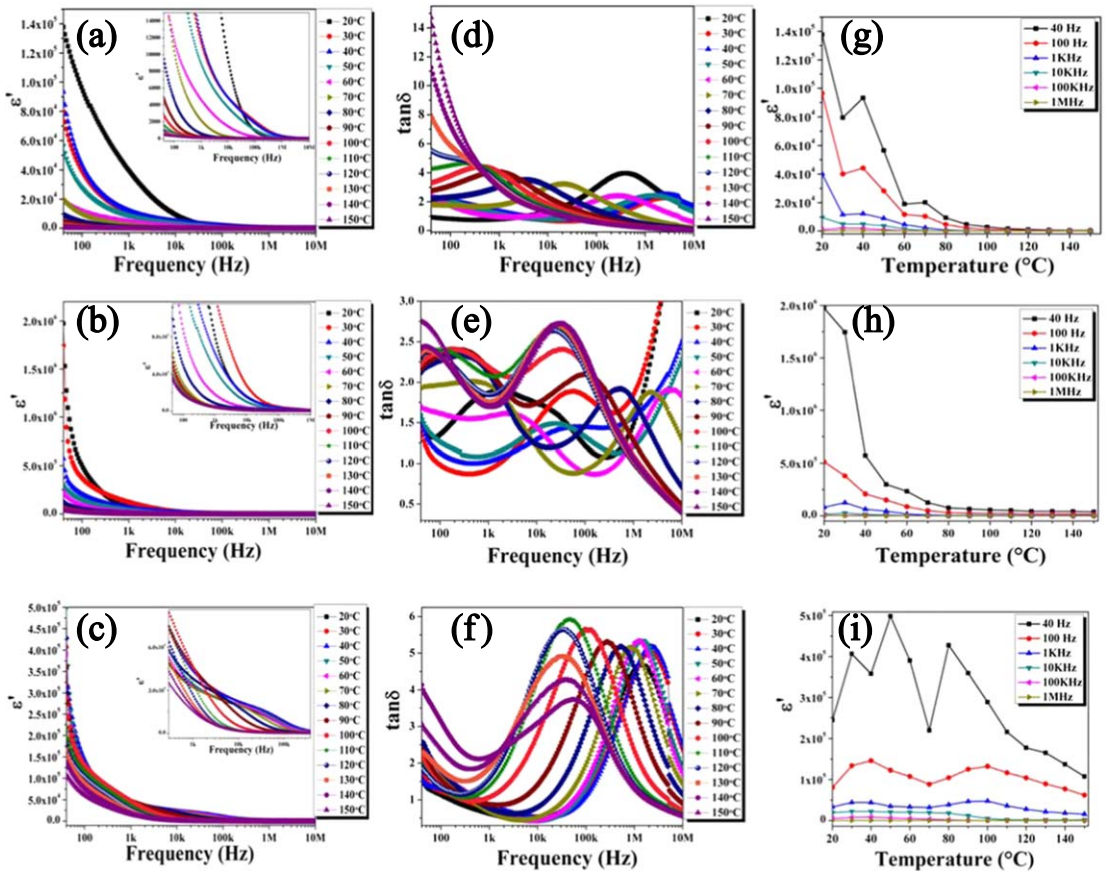


**Figure 7.** Variation of dielectric constant with frequency (a)–(c), tangent loss (d)–(f) and temperature dependent dielectric response (g)–(i) for the samples NBH, GBH and CBH respectively.

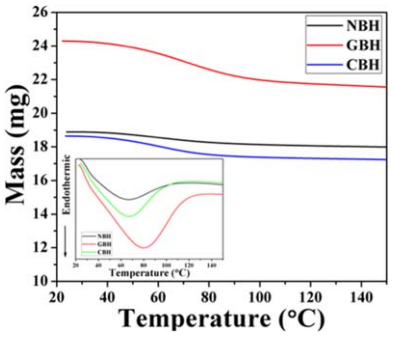


**Figure 8.** Temperature mediated mass losses (TGA) and differential thermal analyses (DTA) (inset) of the samples.

In all three samples, there was a drastic reduction of dielectric constant value with increasing frequency. The values of the dielectric constant at lower frequency were considerably higher due to the Maxwell-Wagner interfacial polarization effect [50, 51], which is in good agreement with Koop's theory [52]. As per this theory, the conducting grains of the dielectric medium are separated by poorly conducting grain boundaries which are formed due to imperfection in crystal alignment. Doping of larger sized ions like $Gd^{3+}$ and $Cu^{2+}$ causes crystal defects, as evident from our XRD results. These defects generate space charge distributions at the interfaces. Space charge comes under the influence of the external field and trapped at interfacial defects centers on grain boundary during their movement and converted into dielectric species that result in high dielectric constant in our doped samples [53, 54].

On the other hand, incorporation of larger sized Gd-ions into the boehmite matrix causes higher stress, resulting in nearly rod-shaped morphology that enhances the surface to volume ratio and results in the highest value for dielectric constant ($1.973 \times 10^6$) at room temperature and 40 Hz frequency. A lower amount of

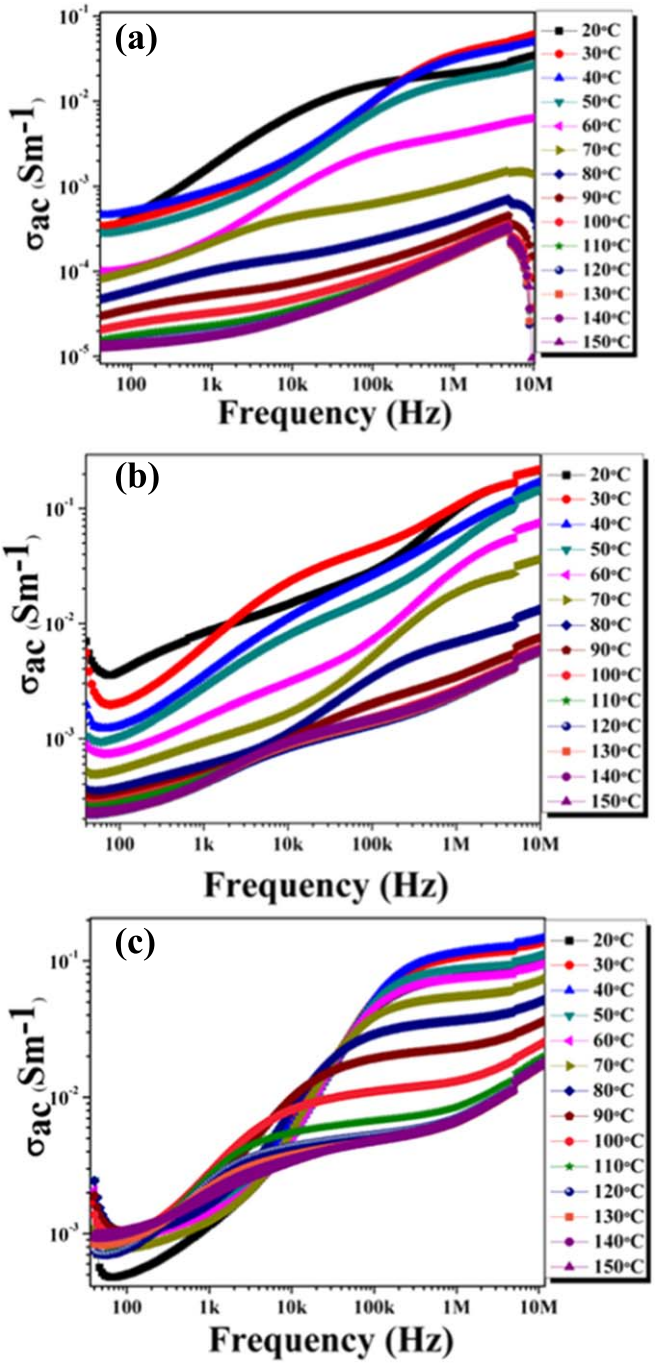


**Figure 9.** Variation of ac electrical conductivity with frequency for different temperatures of the samples (a) NBH, (b) GBH, (c) CBH.

microstrain developed due to the incorporation of copper ions which further creates rhomboidal particles with a surface area of 5.282 $m^2\ g^{-1}$ and causes a dielectric constant of $4.07 \times 10^5$, while for NBH, it was found to be lowest ($1.37 \times 10^5$).

In reality, the enhanced surface to volume ratio can accommodate a higher number of electric dipoles dielectric species that further can enhance the permittivity value as we have mentioned herein. Henceforth, the dielectric constant of our doped samples enhanced not only due to the crystal defects but also due to the higher surface to volume ratios.

Tangent losses of our synthesized nanostructures are in good agreement with high dielectric values. In every case, the peaks of the loss tangent shift toward the lower frequency sides with increasing temperatures (figures 7(d)–(f)). This is because, at higher temperatures γ-AlOOH (boehmite) turns into another unstable phase ($\gamma^*$-AlOOH) that has more oxygen vacancies [55]. These vacancy defects contribute to higher values of the tangent loss in the low-frequency regions and at high temperatures.

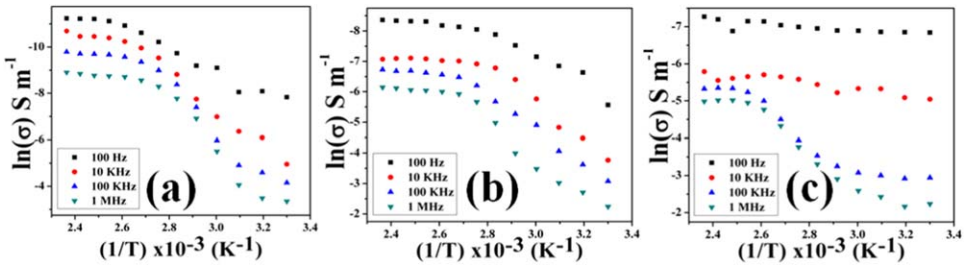


**Figure 10.** Arrhenius plots for the samples (a) NBH, (b) GBH and (c) CBH at different frequency domain.

**Table 5.** Calculated Activation energies ($E_a$) from Arrhenius plots.

| Sample name | Frequency | $E_a$(eV) |
|---|---|---|
| NBH | 100 hz | 0.5135 |
| | 10 kHz | 0.7301 |
| | 100 kHz | 0.9028 |
| | 1 MHz | 0.9728 |
| GBH | 100 hz | 0.2658 |
| | 10 KHz | 0.6803 |
| | 100 KHz | 0.7248 |
| | 1 MHz | 0.784 |
| CBH | 100 Hz | 0.0428 |
| | 10 KHz | 0.0976 |
| | 100 KHz | 0.4001 |
| | 1 MHz | 0.5281 |

The permittivity graphs plotted against varying temperatures have been depicted in figures 7(g)–(i) which illustrates that the dielectric value is quite high for NBH and GBH up to 70°–80 °C temperatures and then slowly decreases. Thermo-gravimetric analysis (TGA) and Differential Thermal Analysis (DTA) have been performed to investigate this phenomenon (figure 8). Very small amount of samples have been placed into platinum crucibles and the TGA-DTA were performed in presence of N2 gas as the medium. A DTG-60H, Shimadzu was employed for this purpose with a constant heating rate of 10 °C $min^{-1}$.

TGA-DTA data shows that the mass loss in case of NBH is around 4.796% with an endothermic peak centered at 66.67 °C, whereas, it is 11.157% and 7.453% with peaks centered at 79.92 and 67.17 °C for GBH and CBH respectively. As par our dielectric data suggest, the electrical permittivity also decreases slowly in this particular region due to the release of adsorbed moisture from the surface of the samples. Nonetheless, low mass losses indicate that our samples are quite stable up to 150 °C and applicable for capacitive applications and incorporation of foreign cations increases the thermal stability of our doped samples.

### 3.4. Electrical conduction mechanism

The electrical conductivity of the three nanostructures is investigated to explore the conduction mechanism. From figure 9 it is quite evident that the lower frequency region (<10 kHz) contributes low values of ac conductivity for all the samples as the grain boundary restricts the hopping of the free charge carriers [56]. Beyond the 10 kHz field frequency, the samples exhibit high values of ac conductivities. In the high-frequency domain, charge carriers get their activation energies ($E_a$) to overcome the potential barrier and results in higher values of electrical conductivities. The activation energies of the entire sample set have been calculated by using the Arrhenius equation as follows [57],

$$\sigma = \sigma_0 \, e^{\frac{-E_a}{K_B T}} \tag{3}$$

where $E_a$ is the activation energy, $\sigma_0$ be the pre-exponential factor, $K_B$ is Boltzmann constant and T is the absolute temperature. Arrhenius plots were estimated from the ac conductivity data calculated at field frequencies 100 Hz, 10 kHz, 100 kHz and 1 MHz (figure 10). A detailed depiction of activation energies is given in table 5.

Among the three samples, GBH shows the highest conductivity values at higher frequency region and NBH has the lowest value of ac conductivity among these three samples. In reality, doped samples (GBH and CBH) have a higher surface area and a higher number of free charge carriers which makes them easier to perform hopping from one grain to another under the external electric field frequency. Henceforth, doped boehmite samples, especially GBH have the potential to produce good conduction among the three.

## 4. Conclusion

Here we synthesized transition metal (Cu(II)) and rare earth metal (Gd(III)) decorated boehmite nanostructures and analyzed their structural, microstructural and electrical properties based on crystallographic deformation. This is the first time when the dielectric and conductivity properties of these doped samples along with pure boehmite nanostructure have been performed and compared. Rietveld refinement enables us to perform microstructural analyses that make a crucial impact to study the dielectric and ac conductivity of these nanostructures. Increasing microstrain not only generates crystal defects but also enhances the electrical properties significantly by modulating surface area and morphology. Temperature-dependent variation of electrical parameters of these nanostructures shows that particularly doped samples are electrically stable which was further investigated by using TGA-DTA. Among these three nanostructures, GBH shows a promising value of dielectric constant ($1.97 \times 10^6$ at 40 Hz frequency in room temperature) with a very low tangent loss whereas, copper doped CBH has a high dielectric permittivity with remarkably high-temperature stability. Due to their colossal permittivity, high-temperature stability and negligible tangent loss, these doped boehmite samples could be used as potential materials in energy harvesting devices.

## Acknowledgments

Authors would like to thank the Department of Physics, Jadavpur University, for extending experimental facilities. S B and S D would like to acknowledge DST-SERB (Grant No. EEQ/2018/000747) for funding.

## Notes

The authors declare no conflict of interest.

## Synopsis

This work demonstrates how incorporation of infinitesimally small amounts of transition metal Cu(II) and rare earth metal Gd(III) alters the crystallographic properties of doped boehmite samples and results in the enhancements of temperature stability and electrical properties of the doped boehmite samples.

## ORCID iDs

Shubham Roy https://orcid.org/0000-0001-5245-3229
Dipak Kr Chanda https://orcid.org/0000-0003-0147-4972
Sukhen Das https://orcid.org/0000-0001-8372-3076

## References

[1] Shipway A N, Katz E and Willner I 2000 *Chem. Phys. Chem.* **1** 18–52
[2] Sarkar S and Chattopadhyay K K 2012 *Physica E* **44** 1742–6
[3] Mendoza-Damián G, Tzompantzi F, Pérez-Hernández R, Gómez R and Hernández-Gordillo A 2016 *Catalysis Today* **266** 82–9
[4] Maity A and Panda S K 2018 *AIP Conf. Proc.* (https://doi.org/10.1063/1.5028688)
[5] Yang Y *et al* 2019 *Chinese Chemical Letters* **30** 2065–88
[6] Yang Y *et al* 2019 *Chinese Chemical Letters* **30** 2089–109
[7] Hu Y and Wang Z L 2015 *Nano Energy* **14** 3–14
[8] Xu B, Qi S, Li F, Peng X, Cai J, Liang J and Ma J 2019 *Chinese Chemical Letters* **31** 217–22
[9] Lead J R, Batley G E, Alvarez P J, Croteau M N, Handy R D, McLaughlin M J, Judy J D and Schirmer K 2018 *Environmental toxicology and chemistry* **37** 2029–63
[10] Carretero M I and Pozo M 2009 *Applied Clay Science* **46** 73–80
[11] Oun A A, Shankar S and Rhim J W 2019 *Critical Reviews in food Science and Nutrition* 1–26
[12] Guo S, Dong S and Wang E 2009 *Chem. Eur. J.* **15** 2416–24
[13] Liu J, Ma Q, Huang Z, Liu G and Zhang H 2019 *Adv. Mater.* **31** 1800696

[14] Zhao P, Yao M, Ren H, Wang N and Komarneni S 2019 *Appl. Surf. Sci.* **463** 931–8
[15] Maity A, Samanta S, Chatterjee S, Maiti R, Biswas D, Saha S K and Chakravorty D 2018 *Journal of Physics D: Applied Physics* **51** 245301
[16] Samanta S, Maity A, Chatterjee S, Maiti R, Biswas D, Giri S and Chakravorty D 2019 *Transactions of the Indian Institute of Metals* **72** 1963–9
[17] Ovais M, Khalil A T, Raza A, Islam N U, Ayaz M, Saravanan M, Ali M, Ahmad I, Shahid M and Shinwari Z K 2018 *Appl. Microbiol. Biotechnol.* **102** 4393–408
[18] Hou J, Inganäs O, Friend R H and Gao F 2018 *Nat. Mater.* **17** 119
[19] Gan X, Zhao H, Schirhagl R and Quan X 2018 *Microchimica Acta* **185** 478
[20] Liu X, Yao Y, Ying Y and Ping J 2019 *Trends Anal. Chem.* **115** 187–202
[21] Tsai W T, Nguyen M H, Lai J R, Nguyen H B, Lee M C and Tseng F G *Sens. Actuators, B* **265** 75–83
[22] Dey A 2018 *Mater. Sci. Eng. B* **229** 206–17
[23] Hoque N A, Thakur P, Biswas P, Saikh M M, Roy S, Bagchi B, Das S and Ray P P 2018 *J. Mater. Chem. A* **6** 13848–58
[24] Chen C, Zhang Y, Li Y, Dai J, Song J, Yao Y, Gong Y, Kierzewski I, Xie J and Hu L 2017 *Energy Environ. Sci.* **10** 538–45
[25] He S *et al* 2017 *Carbon* **122** 162–7
[26] Wu D, Zhang W, Feng Y and Ma J 2020 *Journal of Materials Chemistry A.* (https://doi.org/10.1039/C9TA12859J)
[27] Cicciù M, Fiorillo L, Herford A S, Crimi S, Bianchi A, D'Amico C, Laino L and Cervino G 2019 *Biomedicines* **7** 12
[28] Grumezescu A and Oprea A E (ed) 2017 *Nanotechnology Applications in Food: Flavor, Stability, Nutrition and Safety* (New York: Academic)
[29] Štefanić G and Musić S 2011 *Croat. Chem. Acta* **84** 481–5
[30] Haghnazari N, Abdollahifar M and Jahani F 2014 *J. Mex. Chem. Soc.* **58** 95–8
[31] Musić S, Dragčević Đ and Popović S 1999 *Mater. Lett.* **40** 269–74
[32] Bai X, Caputo G, Hao Z, Freitas V T, Zhang J, Longo R L, Malta O L, Ferreira R A and Pinna N 2014 *Nat. Commun.* **5** 5702
[33] Kirchner S, Teychené S, Boualleg M, Dandeu A, Frances C and Biscans B 2015 *Chem. Eng. J.* **280** 658–69
[34] Abram A, Eršte A, Dražić G and Bobnar V 2016 *J. Mater. Sci: Mater. Electron* **27** 10221–5
[35] Wu Z, Zhuo Q, Sun T and Wang Z 2015 *J. Appl. Polym. Sci.* **132** 41409
[36] Solovev Y V, Prilepskii A Y, Krivoshapkina E F, Fakhardo A F, Bryushkova E A, Kalikina P A, Koshel E I and Vinogradov V V 2019 *Sci. Rep.* **9** 1176
[37] Liu G H, Li Z, Li X B, Qi T G, Peng Z H and Zhou Q S 2017 *Int. J. Miner, Metall Mater.* **24** 954–63
[38] Roy S, Pal K, Bardhan S, Maity S, Chanda D K, Ghosh S, Karmakar P and Das S 2019 *Inorg. Chem.* **58** 8369–78
[39] Bunaciu A A, UdriŞTioiu E G and Aboul-Enein H Y 2015 *Crit. Rev. Anal. Chem.* **45** 289–99
[40] Serafini A, Lutterotti L, Gross S and Gialanella S 2017 *Powder Diffr.* **32** S63–8
[41] Das S, Das S, Roychowdhury A, Das D and Sutradhar S 2017 *J. Alloys Compd.* **708** 231–46
[42] Ateia E E, Ahmed M A, Salah L M and El-Gamal A A 2014 *Phys. B* **445** 60–7
[43] Zirehpour A, Rahimpour A, Seyedpour F and Jahanshahi M 2015 *Desalination* **371** 46–57
[44] Brostow W and Datashvili T 2008 *Chem. Chem. Technol.* **2** 27–32
[45] Dandapat A and De G 2010 *J. Mater. Chem.* **20** 3890–4
[46] Zhang J *et al* 2006 *J. Phys. Chem. B* **110** 14249–52
[47] Chanda D K, Das P S, Samanta A, Dey A, Mandal A K, Gupta K D, Maity T and Mukhopadhyay A K 2014 *Ceram. Int.* **40** 11411–7
[48] Chanda D K, Samanta A, Dey A, Das P S and Mukhopadhyay A K 2017 *J. Mater. Sci.* **52** 4910–22
[49] Usha V, Kalyanaraman S, Vettumperumal R and Thangavel R 2017 *Physica B* **504** 63–8
[50] Chuprinko D and Titov K 2017 *Geophys. J. Int.* **209** 186–91
[51] Das S, Das S, Roychowdhury A, Das D and Sutradhar S 2017 *J. Alloys Compd.* **708** 231–46
[52] Koops C G 1951 *Phys. Rev.* **83** 121–4
[53] Hassan A, Mustafa G M, Abbas S K, Atiq S, Saleem M, Riaz S and Naseem S 2019 *Ceram. Int.* **45** 14576–85
[54] Qi X, Sun E, Zhang R, Yang B, Li S and Cao W 2017 *Ceram. Int.* **43** 16819–26
[55] Wang J A, Bokhimi X, Morales A, Novaro O, Lopez T and Gomez R 1999 *J. Phys. Chem. B* **103** 299–303
[56] Kabashima S and Kawakubo T 1968 *J. Phys. Soc. Jpn* **24** 493–7
[57] Sudha L K, Sukumar R and Uma Rao K 2014 *Int. J. Mach. Mach. Mater.* **2** 96–100